ELSEVIER

Journal of Power Sources 91 (2000) 217–223

JOURNAL OF POWER SOURCES

www.elsevier.com/locate/jpowsour

Performance characteristics of zinc hexacyanoferrate/Prussian blue and copper hexacyanoferrate/Prussian blue solid state secondary cells

M. Jayalakshmi, F. Scholz *

Institut für Chemie und Biochemie, Ernst-Moritz-Arndt-Universität Greifswald, Soldmannstraße 23, D-17489 Greifswald, Germany

Received 11 January 2000; accepted 14 March 2000

Abstract

Solid state secondary cells were constructed with Prussian blue (PB), i.e. iron (III) hexacyanoferrate (II) as the active material for cathodes and zinc (II) hexacyanoferrate (III) (Zn*hcf*) and copper (II) hexacyanoferrate (III) (Cu*hcf*) as the active materials for anodes. The metal hexacyanoferrates were mixed with graphite powder, potassium chloride and dilute hydrochloric acid to form a thick paste. A Nafion membrane was used as separator transporting protons only. Charge–discharge studies were carried out using galvanostatic method and double step chronopotentiometric method. The cell voltage at half-discharge for Zn*hcf*/PB cell varied from 0.6 to 0.8 V depending on the discharge rate. For the Cu*hcf*/PB cell, the cell voltage at half-discharge was 0.87 V for a precycled cell and it dropped to 0.75 V after 100 cycles. The practical capacity of the Zn*hcf*/PB cell (12 A h/kg) was higher than that of the Cu*hcf*/PB cell (5 A h/kg), however, the recycling efficiency of the latter was far better than that of the former. Open-circuit voltage decay and recovery transients were recorded for both cells and analysed.

Keywords: Prussian blue; Zinc hexacyanoferrate; Copper hexacyanoferrate; Solid state secondary cells; Charge–discharge studies

1. Introduction

The zeolite-like hexacyanoferrates are known to intercalate alkali metal cations reversibly during the electrochemical redox transformations. The intercalating cations are mobile and they freely move between sites in the hexacyanoferrate (host) lattice. Further, the intercalation–deintercalation cycles are not accompanied by any dissolution of the solid compounds. These two properties are exploited for the application of metal hexacyanoferrates as battery electrodes in electrochemical cells. Such application had been tested by few authors and the results are not successful due to the technical difficulties in handling the material. In the zeolitic matrix of PB, potassium ions in an aqueous electrolyte can be intercalated and deintercalated highly reversibly into the order of 10^5 cycles [1] and 10^7 cycles [2] when electrochemically deposited on ITO and SnO_2 substrates, respectively. Prussian blue is also known to be highly stable in acidic solutions. The high reversibility of two distinct redox reactions of PB involving the reduction of the high spin iron under formation of Prussian white (PW) and the oxidation of the low spin iron under formation of Berlin green (BG) are taken into account for constituting a PB battery with PB as both anode and cathode by V.D. Neff [3] for the first time. Loss of PB as sol from the graphite rod was encountered on repetitive cycling which led to the failure of this cell. In another work, the rechargeability of solid state copper cells by using PB and BG cathodes was studied [4]. The cell voltages of the Cu/PB cell was 0.58 V, and that of the Cu/BG cell was 0.5 V. The maximum discharge capacities at 100 μA/cell were 1.35 and 1.98 mA h, respectively. The Cu/BG cell was reported to be relatively more stable (over 700 cycles) compared to that of Cu/PB cell. In the same lines, PB and BG were tried as cathodes in lithium secondary batteries with an aprotic electrolyte system [5]. The authors concluded that the iron cyanides could be used as a cheap rechargeable cathode since they show electrode potentials and capacities that are comparable to the conventional oxide cathodes. The bottleneck in practical battery use was identified to be due to the presence of water molecules in the structure, which may cause degradation of the lithium or carbon counter electrode, thus leading to safety hazard.

* Corresponding author. Tel.: +49-3834-864450; fax: +49-3834-864451/864413.

E-mail address: fscholz@rz.uni-greifswald.de (F. Scholz).

0378-7753/00/$ - see front matter
PII: S0378-7753(00)00475-4

Some of the derivatives of PB had been tried as battery electrodes in secondary cells. Thin layers of PB (Fe*hcf*) and copper hexacyanoferrate (Cu*hcf*) on platinum were used as anode and cathode in a secondary cell with aqueous potassium nitrate solution as electrolyte [6]. This cell was reported to show degradation due to overcharging the Cu*hcf* layer. In the extended work by the same authors [7], they reported another secondary cell based on thin layers of nickel hexacyanoferrate (Ni*hcf*) on nickel and nickel hexacyanoruthenate (Ni*hcru*) on platinum with sodium perchlorate solution as electrolyte. With increased cycling, solubility of the films was reported to be the reason for the fall in capacity of the cell. However, in both of the above mentioned studies, the base metal used is very expensive and it is not practical to use such noble metals in aqueous batteries.

In our earlier work, we reported the charge–discharge characteristics of a solid state secondary cell with PB as active material for both anode and cathode and Nafion membrane as separator [8]. In order to avoid the leakage of PB as sol on continuous cycling, it was mixed with graphite powder, potassium chloride and dilute hydrochloric acid to form a thick paste forming the battery electrode. Up to 60 cycles carried out, there was no significant deterioration. For the stabilised cell, the cell voltage was invariable 1.0 V at half-discharge. In the present work, we examine the possibility of analogues of PB such as Zn*hcf* (Zinc hexacyanoferrate) and Cu*hcf* (Copper hexacyanoferrate) to be used as battery electrodes in conjunction with PB as cathode in solid state secondary cells, because it was expected that these compounds are at least as suitable as Prussian blue. Cu*hcf* had been tried earlier [6] as battery electrode but not Zn*hcf*. Here, the assembled Zn*hcf*/PB and Cu*hcf*/PB cells are studied by galvanostatic mode for their charge–discharge behaviour. Open-circuit voltage decay and recovery transients are recorded to understand the cell's behaviour in open-circuit conditions. Double step chronopotentiometric studies are carried out to test the cycleability of Cu*hcf*/PB cell. The results of this study show that Zn*hcf* and Cu*hcf* perform considerably worse than Prussian blue. This unfortunate result points to the search of improved electrode materials, e.g. solid solution hexacyanoferrates (mixed metal hexacyanoferrates) and to material of even less crystallinity than the studied one.

2. Experimental

2.1. Chemicals

Commercial PB powder was used as obtained (HEYL chem.-pharm. Fabrik, Berlin, Germany). The powder X-ray diffraction pattern of the PB was that of insoluble form of PB, $Fe_4^{III}[Fe(CN)_6)_3]$ as reported, except for minor differences in the diffraction intensities. Graphite powder used as an auxiliary conductive agent was of analytical grade. Potassium chloride used along with PB and graphite powder was also of analytical grade and used as obtained.

Zinc(II) hexacyanoferrate(III) was synthesised by dropwise addition of a solution of hexacyanoferrate salt (25 mmol $K_3[Fe(CN)_6]$ in 50 ml H_2O) into a stirred solution of zinc sulphate (25 mmol $ZnSO_4 \cdot 7H_2O$ in 50 ml H_2O). The pale green precipitate was filtered off, washed with water and dried at 80°C.

Copper(II) hexacyanoferrate(III) was also prepared by dropwise addition of a solution of hexacyanoferrate (III) (25 mmol $K_3[Fe(CN)_6]$ in 50 ml H_2O) into a stirred solution of copper sulphate (25 mmol $CuSO_4 \cdot 6H_2O$ in 50 ml H_2O). The dark green precipitate was filtered off, washed with water and dried at 80°C.

2.2. Preparation of battery electrodes

For the Zn*hcf*/PB secondary cell, the cathode (PB) and anode (Zn*hcf*) were made as per the procedure followed in our earlier work [8]. The cathodic mixture consisted of PB powder (0.25 g), graphite powder (1.1 g) and potassium chloride (0.25 g). This mixture was well ground in an agate mortar to form a paste with a few drops of diluted hydrochloric acid (0.1 M). The electrode mixture was then filled into a circular disc and the resultant electrode had a diameter of 14 mm and thickness of 4 mm. The anodic mixture consisted of Zn*hcf* powder (0.25 g), graphite powder (1.1 g) and potassium chloride (0.25 g). Similarly, this mixture was well ground in an agate mortar to form a paste with a few drops of diluted hydrochloric acid (0.1 M). The paste was then filled into a circular disc and the resultant electrode had the same dimensions as that of anode.

For the Cu*hcf*/PB secondary cell, the cathode (PB) was prepared in the similar fashion as mentioned above. The anodic mixture consisted of Cu*hcf* powder (0.25 g), graphite powder (1.1 g) and potassium chloride (0.25 g). With a few drops of diluted hydrochloric acid (0.1 M), the mixture was ground well into a paste and filled into a circular disc to form a battery electrode of dimensions as that of anode.

2.3. Cell design and configuration

The Zn*hcf*/PB and the Cu*hcf*/PB secondary cells had the configurations PB_m/Nafion/Znhcf_m and PB_m/Nafion/Cuhcf_m where the subscript 'm' denotes the mixture of electroactive material, graphite and KCl. Fig. 1 shows the cross-sectional view of the cell designed. Electrical

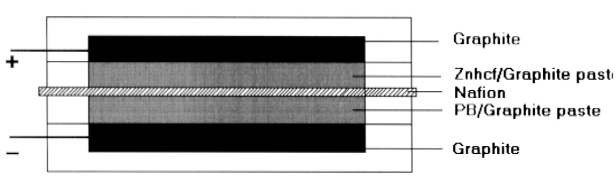

Fig. 1. Cross-sectional view of the Zn*hcf*/PB solid state secondary cell.

contact is made by graphite (14 mm diameter, 4 mm thick) embedded into a polyacrylic block with dimensions of 24×24 mm and 6 mm thickness. Nafion sandwiched between the two electrodes acted as a separator. Nafion also acted as an ion-exchange membrane, exchanging protons between the two electrodes, thus maintaining the charge balance and the insolubility of reduced and oxidised PB, Zn*hcf* and Cu*hcf*. Although only protons are transported through the separator, the intercalating and deintercalating ions in the active material are potassium ions only.

2.4. Instrumentation

The cells are charged in the galvanostatic mode with an Autolab (ECO-Chemie, Utrecht, Netherlands). They are discharged by using a resistor, voltmeter and multimeter by constant current discharge. The duration of each charging was 30 min and the cycling was performed without rest time. The change in cell voltage during charging and discharging was measured at intervals of 5 min.

3. Results and discussion

3.1. Znhcf / PB secondary cell

Fig. 2 shows the cyclic voltammograms of PB and Zn*hcf* to give a clear perception about the redox states in these two iron cyanide materials. When the Zn*hcf*/PB secondary cell is charged, Zn*hcf* undergoes reduction as the low spin iron in the +3 oxidation state is reduced to the +2 state, accompanied by the intake of a potassium ion while PB undergoes oxidation as the low spin iron in the +2 state gets oxidised to the +3 state accompanied by the release of a potassium ion. During discharge, the polarity reversal takes place and the reactions proceed in the opposite directions. The half-cell reactions and the net cell reaction can be written as the following.

Charging:

$$\underset{\text{PB}}{\mathrm{KFe^{III}[Fe^{II}(CN)_6]}} \rightarrow \underset{\text{BG}}{\mathrm{Fe^{III}[Fe^{III}(CN)_6]}} + \mathrm{K^+ + e^-} \quad (1)$$

$$\mathrm{KZn^{II}[Fe^{III}(CN)_6] + K^+ + e^- \rightarrow K_2Zn^{II}[Fe^{II}(CN)_6]}. \quad (2)$$

Cell reaction:

$$\mathrm{KFe^{III}[Fe^{II}(CN)_6] + KZn^{II}[Fe^{III}(CN)_6] \rightarrow Fe^{III}[Fe^{III}(CN)_6] + K_2Zn^{II}[Fe^{II}(CN)_6]}. \quad (3)$$

Discharging:

$$\underset{\text{BG}}{\mathrm{Fe^{III}[Fe^{III}(CN)_6]}} + \mathrm{K^+ + e^- \rightarrow} \underset{\text{PB}}{\mathrm{KFe^{III}[Fe^{II}(CN)_6]}} \quad (4)$$

$$\mathrm{K_2Zn^{II}[Fe^{II}(CN)_6] \rightarrow KZn^{II}[Fe^{III}(CN)_6] + K^+ + e^-}. \quad (5)$$

Cell reaction:

$$\mathrm{K_2Zn^{II}[Fe^{II}(CN)_6] + Fe^{III}[Fe^{III}(CN)_6] \rightarrow KZn^{II}[Fe^{III}(CN)_6] + KFe^{III}[Fe^{II}(CN)_6]}. \quad (6)$$

Prior to charging, the Zn*hcf*/PB cell showed an open circuit voltage (OCV) of 0.56 V. This OCV is susceptible to changes depending on the change in composition of either PB or Zn*hcf*. Considering this positive OCV as an advantage, the efforts to discharge the cell without prior charging failed since the cell dramatically deteriorated in terms of current and voltage. Hence the cell has to be initially charged to get it discharged. To calculate the C rate, the equivalent weight of the so-called 'soluble' form of PB, $KFe[Fe(CN)_6]$ (306.8 g/mol) and that of Zn*hcf* $KZn[Fe(CN)_6]$ (316.3 g/mol) was used. ('Soluble' $KFe[Fe(CN)_6]$ is the established term for a $KFe[Fe(CN)_6]$ which, in the absence of an electrolyte, is easily peptised. However, under our experimental conditions it is solid and insoluble due to the presence of an electrolyte.) In the present case, for a weight of 0.25 g of PB and 0.25 g of Zn*hcf* taken to construct cathode and anode, the rate *C* for

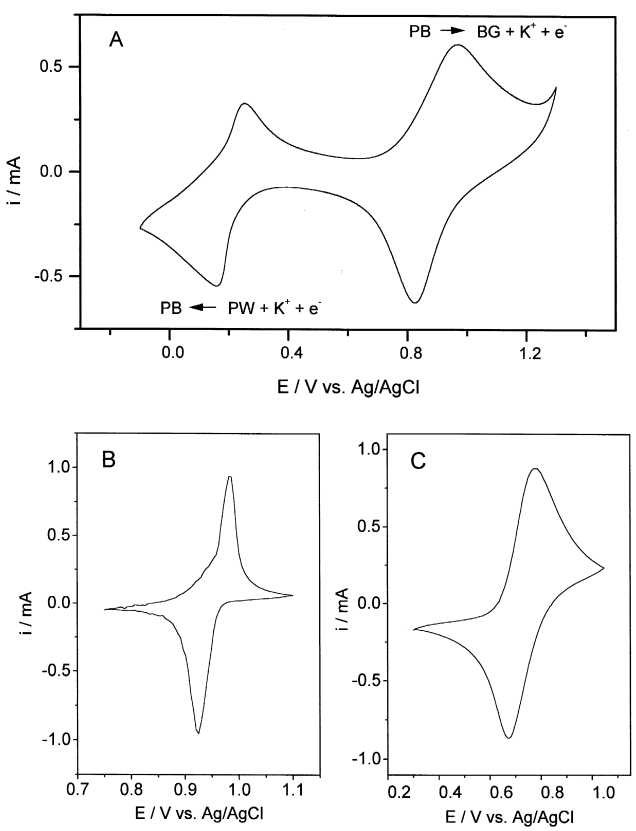

Fig. 2. Cyclic voltammograms of (A) Prussian blue, (B) Zn*hcf* and (C) Cu*hcf* immobilised on a graphite electrode and using a KCl electrolyte.

the Zn*hcf*/PB cell is calculated to be 0.086 as for the charging period of 30 min. The charge–discharge curves of the Zn*hcf*/PB stabilised secondary cell is shown in Fig. 3. In this figure, curves a, b, c represent the charging curves at $C/6$ rate while curves a*, b*, c* represent the discharge curves at $C/7$, $C/9$ and $C/11$ rates, respectively. In the charging curve a (cycle 15), the terminal voltage reached at the end of a charging period of 30 min is 2.4 V, but the discharge curve a* starts only at 1.58 V even though the discharge is carried out without rest time. The case is similar in the other two curves b and c. Another noticeable feature in the charging curves is the difference in terminal voltage reached in each case. In the curve a recorded at cycle 15, it is 2.4 V; in the curve b recorded at cycle 20, it is 2.6 V; in the curve c recorded at cycle 30, it is 3.0 V. There is an increase in terminal voltage with continuous cycling even if the cell is discharged at lower rates. This suggests that the discharge products are resistive, which tend to be cumulative with cycling. Hence, with continuous cycling, the cell needs higher charging rates in order to bring back the cell to original condition. The discharge curves do not show any significant difference in the voltage vs. Q plots and the cell voltage varied from 0.6 to 0.8 V at half-discharge, depending on the rate of discharge.

Fig. 4 presents the discharge curves obtained for the Zn*hcf*/PB secondary cell at low discharge current of 2 mA. The curves a, b and c in Fig. 4 show the change in cell voltage with discharge capacity of the cell with cycling. Curve a represents that of the 4th cycle, curve b that of the subsequent 5th cycle while curve c that of 30th cycle. The cell voltage at half-discharge vary significantly with cycling as it can be seen that it was 0.8 V in curve a, 0.6 V in curve b and 0.4 V in curve c. It is known that if the cells are discharged slowly at constant current, then this procedure gives results sufficiently close to equilibrium. An interesting feature observed in the discharge

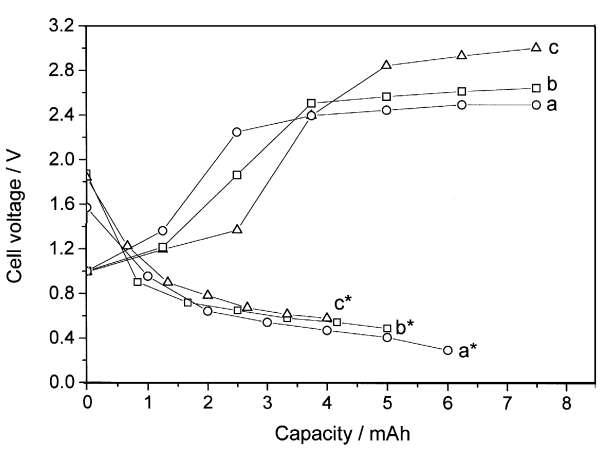

Fig. 3. Charge–discharge curves of the stabilised Zn*hcf*/PB cell for three cycles (1) a, a*, (2) b, b* and (3) c, c* at $C/6$ charge rate and $C/7$,$C/9$,$C/11$ discharge rates, respectively.

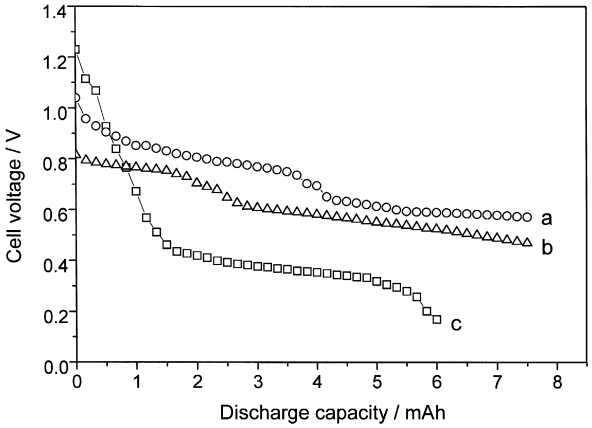

Fig. 4. Discharge curves of the Zn*hcf*/PB cell at a current drain of 2 mA at three different cycles: (a) cycle 1, (b) cycle 2 and (c) cycle 30.

curves a and b was the occurrence of a second plateau followed by the abrupt change in cell voltage around 0.8 and 0.73 V, respectively in both the cases. Such a second plateau was observed and reported in the discharge curves in non-aqueous secondary battery employing PB as cathode [5]. The most plausible reason for the appearance of two plateau regions in the discharge curves a and b can be given as follows: as discharge proceeds, the oxidation of Zn*hcf* electrode is limited to the low spin iron which is oxidised from $+2$ to $+3$ state (cf. Eq. (4)) whereas the simultaneous reduction of PB electrode can proceed beyond BG → PB (cf. Eq. (5)) conversion to another step as

$$\underset{\text{PB}}{\mathrm{KFe^{III}[Fe^{II}(CN)_6]}} + \mathrm{K^+} + \mathrm{e^-} \rightarrow \mathrm{K_2}\underset{\text{PW}}{\mathrm{Fe^{II}[Fe^{II}(CN)_6]}}. \quad (7)$$

In this case, the net cell reaction is

$$\mathrm{K_2Zn^{II}[Fe^{II}(CN)_6] + KFe^{II}[Fe^{III}(CN)_6]} \rightarrow \mathrm{KZn^{II}[Fe^{III}(CN)_6] + K_2Fe^{II}[Fe^{II}(CN)_6]}. \quad (8)$$

Thus, the appearance of the first plateau is due to the reduction of BG to PB and the second plateau is due to the subsequent reduction of PB to PW. The absence of such distinction in curve c may be due to the restriction in rechargeability to the product PB rather than BG. In such a case, the charge–discharge process is limited to the PB ↔ PW transformation.

3.2. Cuhcf / PB secondary cell

The cyclic voltammogram of Cu*hcf* shows a single set of redox peaks due to the redox transition of low spin iron (Fig. 2). This redox reaction is exploited for battery application. The reactions taking place during charge and discharge of Cu*hcf*/PB secondary cell are similar to that written for Zn*hcf*/PB secondary cell, except that Cu re-

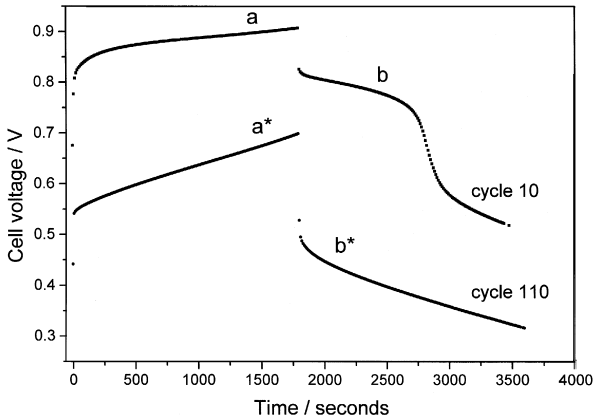

Fig. 5. Double step chronopotentiometric curves obtained for the Cu*hcf*/PB cell (a) by applying 5 mA positive current at cycle 10 (a*), at cycle 110 (b) by applying 5 mA negative current at cycle 10 (b*) at cycle 110 in the time scale of 1800 s for each step.

places Zn in PB analogue. The net cell reaction for charge–discharge process is,

$$KFe^{III}[Fe^{II}(CN)_6] + KCu^{II}[Fe^{III}(CN)_6] \rightleftarrows Fe^{III}[Fe^{III}(CN)_6] + K_2Cu^{II}[Fe^{II}(CN)_6].$$

Fig. 5 shows the double step chronopotentiometric curves obtained for Cu*hcf*/PB cell in pre-cycled and cycled conditions. In this figure, curves a and a* are obtained by passing a positive current of 5 mA to the cell for a period of 30 min. Charging of the cell takes place in this forward step of double step chronopotentiometric experiment. Curves a and a* represent charging curves at cycle 10 and 110, respectively. The reverse step of passing a negative current of 5 mA is similar to a discharge process. This step produces a polarity reversal and the reactions proceed in the opposite direction. Curves b and b* in Fig. 5 represent discharge curves. As can be seen, at the 10th cycle, the cell voltage at half-discharge in curve b is 0.78 V while it decreased to 0.40 V at 110th cycle. The interesting feature in the discharge curve b is the appearance of a second plateau. This step is similar to that observed in Zn*hcf*/PB cell where it is attributed to PB to PW conversion. In curve b* in which case the cell is well cycled, there is no second plateau indicating the restriction in rechargeability to the final product to BG. Again the case is similar to Zn*hcf*/PB cell (cf. Fig. 4, curve c). The decrease in cell voltage with cycling suggests the loss of energy density of cell on prolonged use. Also, the coulombic capacity decreases as evidenced by the proportionality in the area under the curves of pre-cycled and cycled conditions.

The formal potential of the couple PB ↔ BG is 1.17 V and that of PB ↔ PW is 0.02 V vs. SHE by considering the solid hexacyanoferrates [9]. The formal potential of redox transition of Zn*hcf* is 0.93 V vs. SHE, as is that of Cu*hcf*. The counter cation considered for charge neutrality is potassium ion as written in the equations but there is also a possibility that protons play the role of charge balancing cations. In such a case of a mixed insertion of protons and potassium ions into the solid hexacyanoferrates, the formal potentials will vary from the case of pure potassium insertion, which would be reflected in cell voltages.

Theoretical capacities of PB, Zn*hcf* and Cu*hcf* are 87.5, 84.7 and 85.2 A h/kg, respectively. For the Zn*hcf*/PB secondary cell, the practical capacity is 12 A h/kg at high rate of discharge (cf. Fig. 3, curve a*) while it is 15 A h/kg at low rate of discharge (cf. Fig. 4, curve b). The practical capacity calculated for the Cu*hcf*/PB cell based on the chronopotentiometric experiments is 5 A h/kg. It could be seen that there is tremendous difference in theoretical and practical capacities of these solid state cells. Lack of 100% electroactivity of the electrode materials and resistivity of discharge products may contribute to this capacity loss. Both the Cu*hcf*/PB and the Zn*hcf*/PB secondary cell have lower practical capacities than the Prussian blue/Prussian blue secondary cell described previously [8]. This is surprising because no principle differences can account for it.

3.3. Open-circuit voltage recovery transients

Open-circuit voltage recovery transients are well exploited for the evaluation of additives in battery electrodes [10,11]. In the present work, recovery of cell voltage after discharge of both Zn*hcf*/PB and Cu*hcf*/PB cells was recorded and analysed. For example, when the Zn*hcf*/PB cell was discharged at a particular rate (cf. Fig. 3, curve a*), the cell voltage started decreasing as evident from the discharge curves and reaches as low values as 0.29 V. As soon as the circuit was disconnected, within 5 min, the cell voltage recovers dramatically to OCV values ranging from 0.6 to 0.75 V depending on the depth of discharge. As OCV represents the thermodynamic equilibrium cell voltage, this voltage recovery may be due to the equilibrium

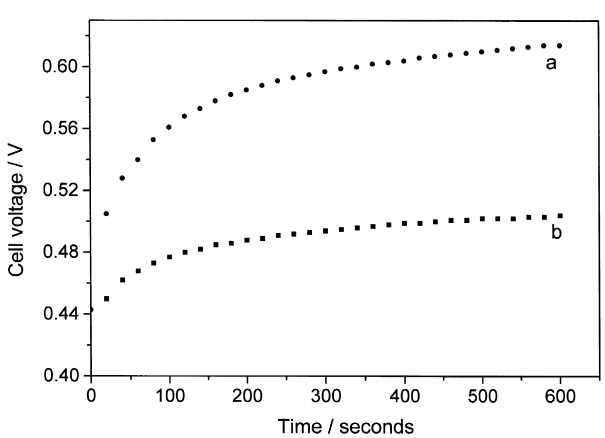

Fig. 6. Open-circuit voltage recovery transients for (a) Zn*hcf*/PB cell and (b) Cu*hcf*/PB cell.

that exists between the unreacted PB and /or Zn*hcf* and the discharge products.

The OCV recovery transients in Fig. 6 highlight this fact. These curves were obtained by noting the change in voltage in the open circuit conditions as soon as the discharge was stopped. The cell voltage reached by Zn-*hcf*/PB cell was 0.6 V while that of Cu*hcf*/PB cell was 0.5 V at the approach of equilibrium values represented by the plateau region. It could be seen that the approach to equilibrium is sluggish in the case of Cu*hcf*/PB cell. This may be due to the enrichment of discharge products on the surface of the active particles of the electrode material. This fact is more clearly observed in the case of Zn*hcf*/PB cell. If the cell was discharged at low rates (cf. Fig. 4, curve c) for longer period, the voltage recovery was increasingly sluggish. The OCV recovered after this experiment (figure not given) was 0.36 V whereas it was 0.6 V after the discharge experiment shown in Fig. 4, curve a. For recharging the cell, the charge required is higher in the former case than in the latter. In general, comparison of performance of both these cells show that the Zn*hcf*/PB cell is more active in voltage recovery than the Cu*hcf*/PB cell. Since the cathode is the same material, the difference in cell voltage and activity arises due to the anode material.

3.4. Open-circuit voltage decay transients

Open-circuit potential decay transients have been determined to understand the processes which occur after switching off the charging before completion. Fig. 7 shows the open-circuit voltage (OCV) decay transient curves obtained for the Zn*hcf*/PB and Cu*hcf*/PB cells. The cells were charged for 30 min under constant current mode by passing an applied current of 15 mA. As soon as the current was switched off, the change in voltage of the cell with time was noted. The fall in voltage was rapid in the initial 4 min and then the cell voltage gets stabilised. As applied current is passed to the Zn*hcf*/PB cell, PB as negative electrode undergoes oxidation and Zn*hcf* as positive electrode undergoes reduction and the cell voltage is the net result of both the reactions. Charging the electrode means a conversion of the hexacyanoferrate particles starting from their surface and advancing into their inner. When charging is stopped the initial potential will be determined by the composition of the outer converted layer. However, the hexacyanoferrates are known to form solid solutions between the different oxidation states [12] and hence it is reasonable to assume that a slow equilibration between the outer converted layer and the inner nonconverted core of the particles occurs. This process will be driven by the activity gradient of the inserted cations and of the different redox forms of iron across the reaction boundary. It could be seen that the stabilised cell voltage at the end of 30 min was 1.1 V for Zn*hcf*/PB cell while it was 0.85 V for Zn*hcf*/PB cell. In this aspect, the Zn*hcf*/PB cell is more beneficial with its higher cell voltage as it adds up to the enhanced energy density of the cell.

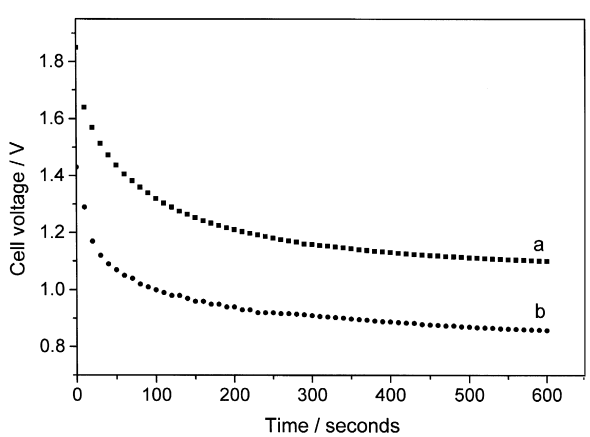

Fig. 7. Open-circuit voltage decay transients for (a) Zn*hcf*/PB cell and (b) Cu*hcf*/PB cell.

4. Conclusions

In search of new active materials for battery applications, Prussian blue and its analogues can be used as alternatives to expensive electrode materials. In this study, we do not pretend that the conditions to construct a commercially viable cell has been optimised, but we do prove that these iron cyanide materials can be used in batteries specifically designed for low currents. Zn*hcf*/PB cell can be more beneficial if it is used as a primary cell whereas Cu*hcf*/PB cell is more advantageous as a secondary cell because of its cycleability. The main advantage in using the iron cyanide materials in battery applications is the non-toxic nature of these compounds and so they are environment friendly. Although being cyanide compounds, they are not hazardous to health; in fact, Prussian blue is used as an antidote for thallium poisoning. The preparation procedure of these iron cyanide compounds is also easier since they can be chemically precipitated and scaled up. The main disadvantages of the hexacyanoferrates studied so far are the obviously too slow kinetics of electrode reactions. This work points to the search for solid solution hexacyanoferrates of low crystallinity with improved ion and electron conductivity.

Acknowledgements

M.J. thanks the Alexander von Humboldt Foundation for the provision of a fellowship. F. Sch. acknowledges support by Fonds der Chemischen Industrie.

References

[1] A. Roig, J. Navarro, J.J. Garcia, F. Vincente, J. Electroanal. Chem. 39 (1994) 437.
[2] K. Itaya, I. Uchida, Acc. Chem. Res. 19 (1986) 162, and references therein.
[3] V.D. Neff, J. Electrochem. Soc. 132 (1985) 1382.
[4] K. Kuwabara, J. Nunome, K. Sugiyama, Solid State Ionics 48 (1991) 303.
[5] N. Imanishi, Y. Takeda, O. Yamamaoto, in: C.F. Holmes, A.R. Landgrebe (Eds.), Batteries for Portable Applications and Electric Vehicles, Proc. Electrochemical Society, Pennington, NJ, USA 97-181997, p. 264.
[6] E.W. Grabner, S. Kalwellis-Mohn, J. Appl. Electrochem. 17 (1987) 653.
[7] S. Kalwellis-Mohn, E.W. Grabner, Electrochim. Acta 34 (1989) 1265.
[8] M. Jayalakshmi and F. Scholz, J. Power Sources, in press.
[9] F. Scholz, A. Dostal, Angew. Chem. 107 (1990) 2876.
[10] N. Jayalakshmi, V.S. Muralidharan, J. Power Sources 32 (1990) 277. J. Power Sources 32 (1990) 341.
[11] K. Vijayamohan, A.K. Shukla, S. Sathyanarayana, J. Power Sources 21 (1987) 53.
[12] N.F. Zakharchuk, N. Naumov, R. Stösser, U. Schröder, F. Scholz, H. Mehner, J. Solid State Electrochem. 3 (1999) 264.